Journal of Earth Sciences and Geotechnical Engineering, Vol. 12, No. 3, 2022, 1-30
ISSN: 1792-9040 (print version), 1792-9660 (online)
https://doi.org/10.47260/jesge/1231
Scientific Press International Limited

Geotechnical Characterization of the Subsurface Using Seismic and Electrical Resistivity Techniques in Mikinduri Meru County, Kenya

Masinde Wechuli[1], Ambusso Willis[1], Githiri Gitonga[2], Barasa Makoha[1] and Kiama Duncan[1]

Abstract

Geotechnical study of the Mikinduri area was conducted with the aim to establish the causes of landslides and ground subsidence during the heavy rainfall. Sounding curves, travel time curves, 2D geoelectric sections, and 2D seismic models revealed 3-5 lithologic units to a depth of 30-250m. The study established thick loose alluvium deposits mixed with clay to a depth of 0.3-15m on an impermeable sub-basement as the possible major trigger of the landslides witnessed during rainy seasons. The thick alluvium deposits are due to erosion. They have been transferred by the location of the Mikinduri area, which lies in the lower regions of the Nyambene domes. Geologically, the domes were formed during Mount Kenya volcanic series and parasitic activities between the early Miocene and late Pleistocene eras. Resistivity modeling revealed deep geologic structures, including possible intrusions extending from 50m deep and faulted regions to a depth of 60-150m in the central and northeast area of study. The faulted area is highly saturated, as revealed by the low resistivity values. The delineated top black cotton soils and alluvium deposit are 40-50% clay and have poor foundation bearing capabilities. In contrast, compacted gravel, silt, and compact basaltic rock basement have good foundation capabilities.

Keywords: Geotechnical, characterization, subsurface, seismic, electrical resistivity, foundation, geoelectric layer, Mikinduri Meru, Kenya.

[1] Kenyatta University, Department of Physics P.O. Box 43844, Nairobi, Kenya.
[2] Jomo Kenyatta University of Agriculture and Technology, Department of Physics P.O. Box 62000-00200, Nairobi, Kenya.

Article Info: *Received:* September 14, 2022. *Revised:* October 30, 2022.
Published online: November 17, 2022.

1. Introduction

Mikinduri area lies between Meru town on the north, Maua town on the south, Kunati town on the east, and Kianjai town on the west. The town is growing rapidly due to its strategic location, increasing population and administrative functions being the headquarter for Tigania's central sub-county. However, the Mikinduri area has been experiencing landslides during heavy rainfall seasons, accompanied by structural failure leading to loss of property and life.

An early study of the geology of the Meru-Isiolo area was done by Mason (1953). The study revealed that the Tigania area, where Mikunduri town is located, is at the boundary of lowlands and the ranges of Nyambene domes (Abuga et al., 2013). The ranges of Nyambene domes stretch in one direction from the Mt. Kenya foothills, and the elevation of the domes is 7000 feet at its peak. The basement is made of basaltic rocks. The area also has black cotton soils, kurkar silts, and gravel (Benson, 2016). Mikinduri area geological setup is similar to the broad geology of the Nyambene area. The physical features of the study area are hills and valleys. The lowlands of the region have thick alluvium deposits due to erosion.

This study was undertaken to investigate the causes of the mass flow observed during the heavy rainfall seasons. It also sought to identify areas with thick loose alluvium deposits and fractured zones and characterize the subsurface in terms of hosting or bearing capabilities. The effects cited for failure of engineering structures include poor quality of building materials and old age structures, but the less frequently mentioned reason is the subsurface conditions of the ground on which the engineering structures are sited (Oluwakuse and Adeyemo, 2020).

Before designing the foundation of a structure, it's vital to ascertain the suitability and the bearing/hosting capacity of the subsurface and the overall geology of the site (Delgado et al., 2000). Geological features and conditions beneath the surface, such as voids, conduits, fractures, nearness of water table to the surface, depth to the bedrock, and expansive clay soil layers, are some prominent risks to the foundation of a building (Andrews et al., 2013).

The application of geophysical methods in geotechnical investigations in the Mikinduri area can bring out the subsurface image of a construction site which is essential to the civil engineer in the design of the foundation of the engineering structures.

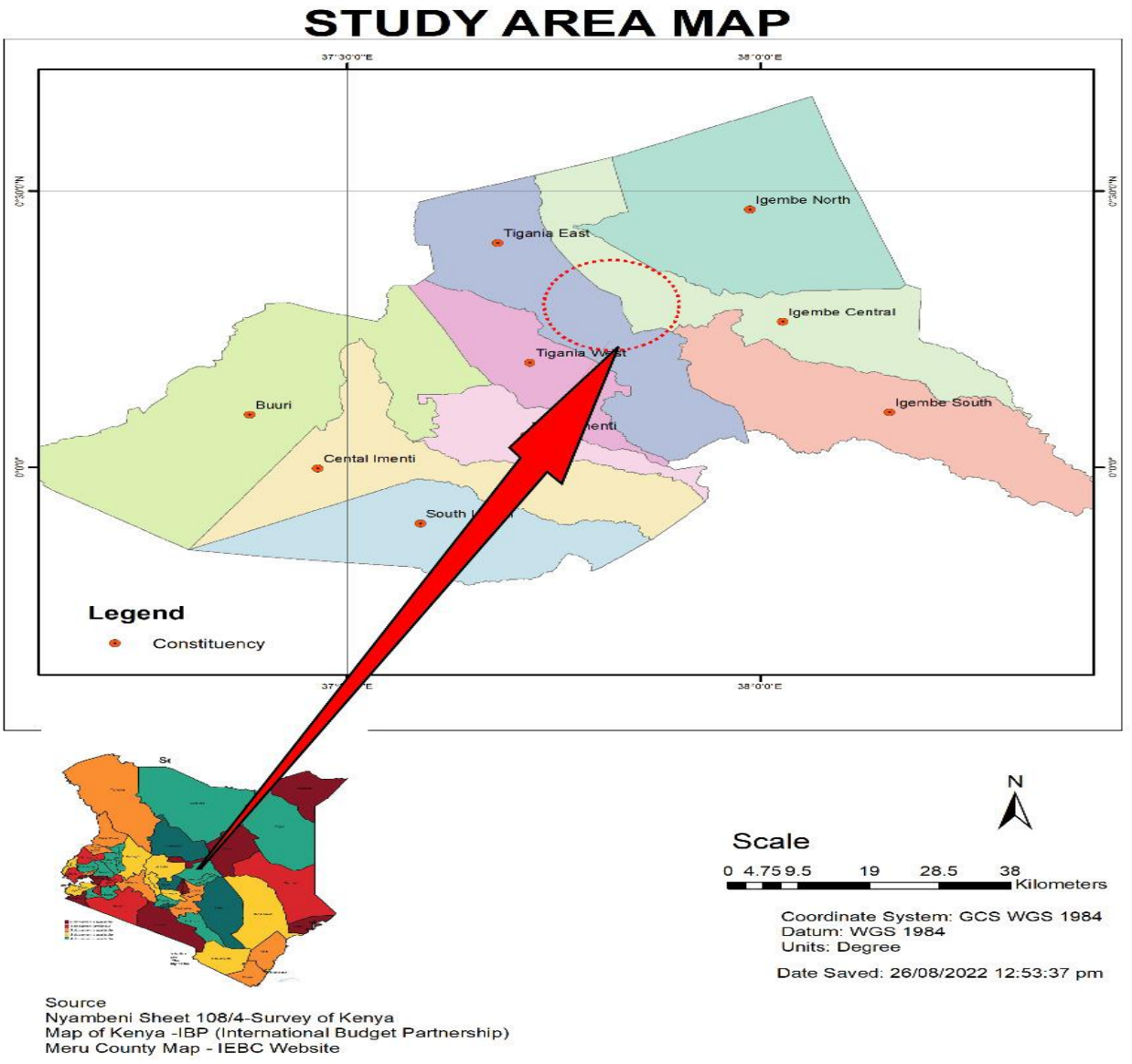

Figure 1: Location of the study area (Nyambeni Sheet 108/4-Survey of Kenya, 1970).

2. Field measurements

The two geophysical techniques used in this study were electrical resistivity and seismic refraction. Geotron resistivity meter MODEL G41 was used to acquire resistivity data, while the Geometrics ES-3000 seismograph was used to obtain seismic data. Seismic data were obtained in open fields with no physical barriers. On the other hand, electrical resistivity Wenner measurements were done along roads to evade physical obstacles like buildings, thick vegetation cover, and challenging terrain. However, limited VES data points were randomly located based on regions with low and high resistivity values, as depicted by the Wenner resistivity contour map shown in Figure 3.

2.1 Electrical resistivity survey

The electrical resistivity field measurements involved VES and Wenner profiling. The electrode separation distance (AB/2) applied was between 1.6 m to 250.0 m for VES. Four Wenner horizontal profiles of each 1000 m in length with $a = 50.0m$ and spaced 1000 m apart were established along the northings, with eight stations on each profile, making 32 stations. All the sounding stations were geo-referenced using Garmin 12 channel personal navigator (GPS) unit, and Universal Transverse Mercator (UTM) positioning format was used. The results were interpreted using IPI2WIN software and Surfer software, which generated pseudo sections, cross-sections, sounding curves, and contour maps for qualitative and quantitative analysis.

2.2 Seismic survey

Geometrics ES-3000 Seismograph was used for the acquisition of seismic data. The frequency was set at 10Hz. Geophones were spaced at 3 metres. The energy source was from a sledgehammer impact on a metal plate placed firmly on the ground surface

Five shots were obtained per spread: the first shot was normal within a 34.5 m (half of the entire length of the spread) distance before geophone 1 (geophone one at zero m). The last shot was a reverse shot at 103.5 m from the first geophone, other shots included forward and reverse end shots at -1.5 m and 70.5 m, respectively, and the centre shot (34.5 m). The length of every seismic profile was 69.0 m, containing 24 geophones. This geometry provides sufficient coverage to produce seismic refraction to a depth of 35.0 m.

2.3 Spatial distribution of VES points and seismic spread lines

Ten vertical electrical sounding stations were established in the study area in low and high resistivity regions, as depicted by the Wenner resistivity contour map in Figure 3. The VES points are from VES 1 on the far southwest in red dots, to VES10 on the far north-east, and seismic spreads lines S1, S2, and S3, shown in black lines, were distributed as shown in Figure 2, and ten Schlumberger soundings with electrode separation (AB/2) between 1.6 m to 250.0 m were employed in data

collection while the seismic investigation was to a depth of 35 m.

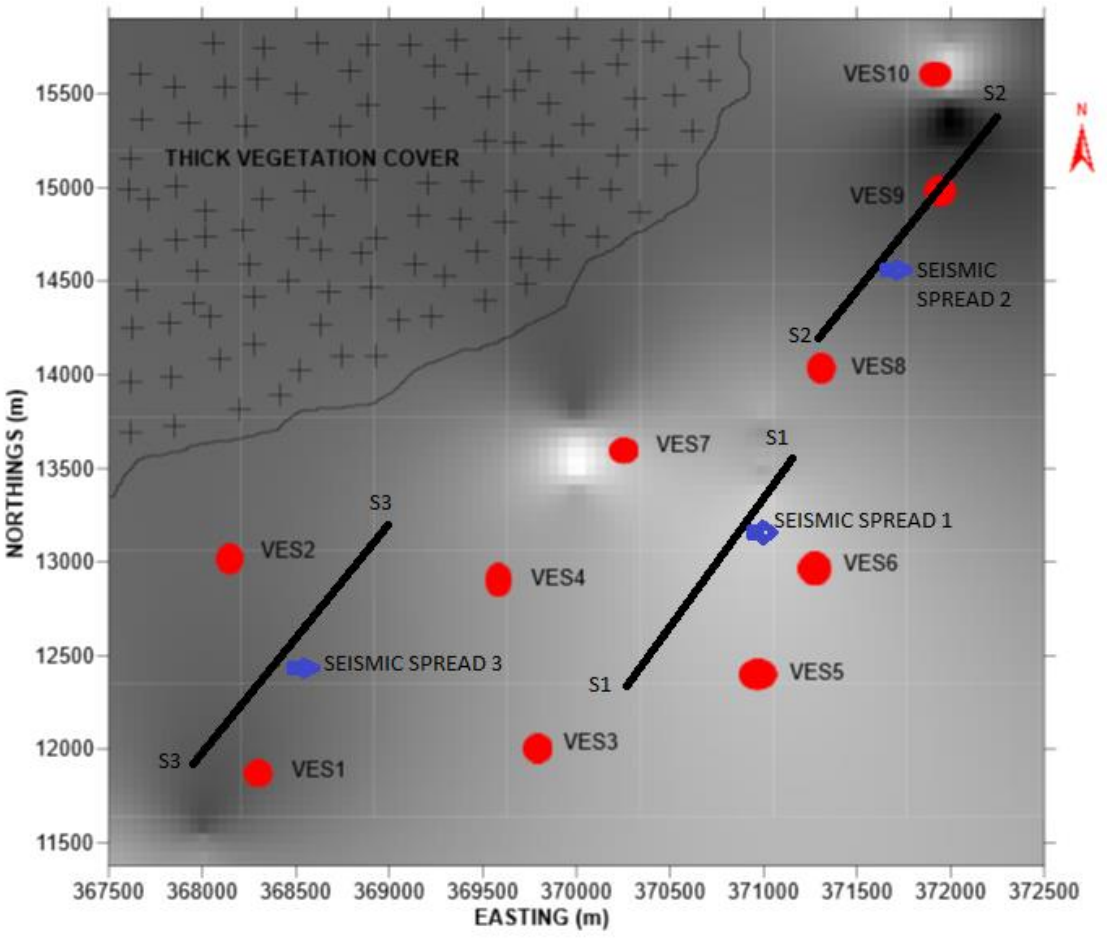

Figure 2: Spatial distribution of VES points and seismic spread lines.

3. Results

3.1 Electrical resistivity

Figure 3 shows the Wenner resistivity contour map, which revealed the resistivity anomalies. The first anomaly was noticed in the far northeast with closely packed contours. The blue represents a region of low resistivity of 50–100 Ωm. Similarly, the central area of study also shows anomalies with closely packed contours, and the red-purple colour represents regions of high resistivity with values ranging between 290-400 Ωm. The southeast area region reveals a part of uniform resistivity of between 230-250 Ωm.

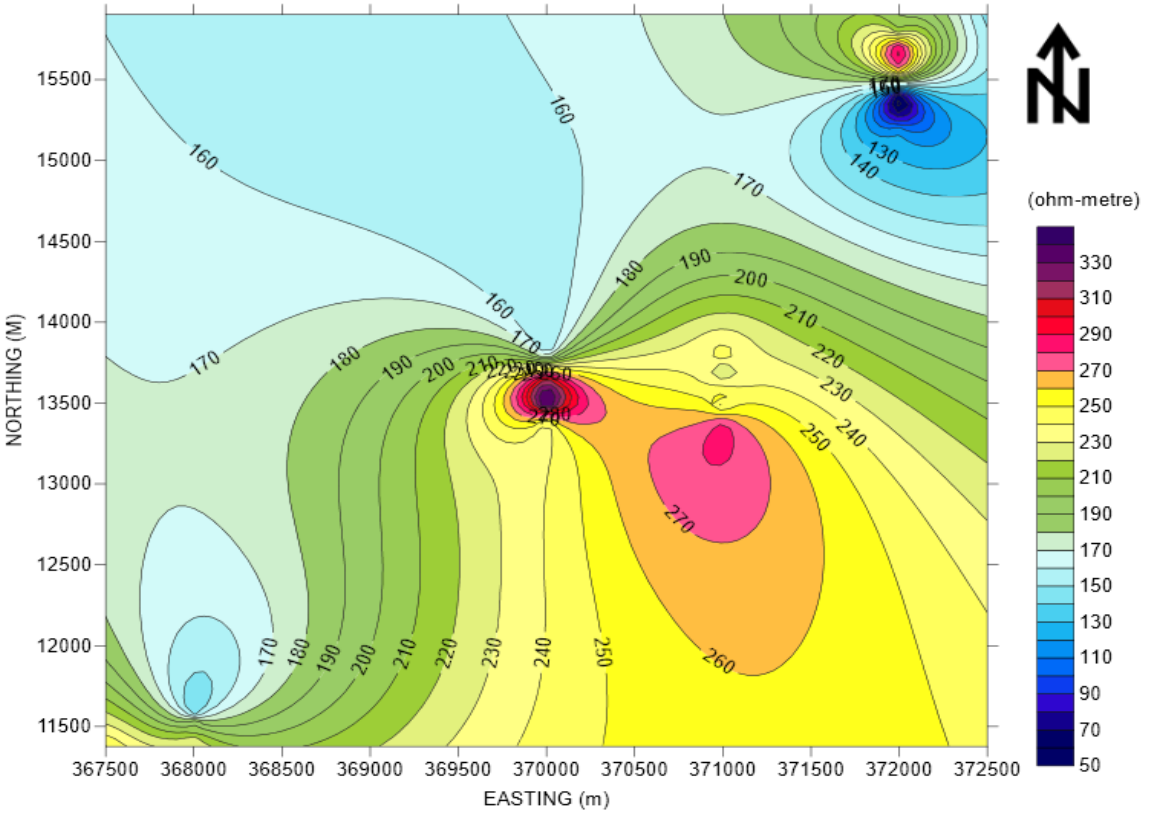

Figure 3: Contour map for Wenner profiles.

3.2 Pseudo-cross-section and resistivity cross-section

Pseudo and resistivity cross-sections for VES1, VES2, VES3, VES4, and VES5 are shown in Figure 4. VES1 shows the presence of 3 geoelectric layers. Similarly, the 2D seismic models in Figures 18,19, and 20 revealed three acoustic layers to a depth of 35m. The basement for the geoelectric layers for VES1 is shallow at a depth of 4.5m with resistivity values 30-50 Ωm, indicating a highly clayey basement with poor foundation-bearing capabilities. The 2nd layer is about 2 m thick with resistivity values 5000-8500 Ωm, revealing a compact sub-basement that is good in foundation bearing. Topsoil is 2 m thick with resistivity values180-290 Ωm, indicating a surficial deposit with a mixture of clay, sand, and silt. The layer is poor in terms of foundation-bearing capabilities.

VES2 shows the presence of 5 geoelectric layers, the basement being the fourth layer at a depth of 13m and is 41m thick with resistivity values 8-20 Ωm, indicating a highly fractured and saturated basement not suitable for super structures. The sub-basement is at a depth of 5m and is 8m thick with resistivity values 2000-3000 Ωm, indicating a compact sub-basement with good foundation-bearing capability. The

second layer is at a depth of 0.5 m and is 5 m thick with resistivity values of 200-350 Ωm and an indication of gravel mixed with sand, clay, and silt. The layer has moderate bearing capability, and the top layer is 0.5 m thick with a resistivity of 20-30 Ωm, indicating soft/expansive clay with extremely poor bearing capabilities and should be excavated.

Four geoelectric layers are revealed from VES3. The shallow basement is the third layer at a depth of 3.5 m. It is 67 m thick with resistivity values 600-1200 Ωm, indicating that compacted gravel and sand have good foundation-bearing capabilities. The second layer of VES3 is at a depth of 0.7 m. It is 3 m thick with a resistivity of 5000-8500 Ωm, indicating a solid compact sub-basement with high foundation bearing capabilities. The top layer is 0.7 m thick with a resistivity of 10-20 Ωm, showing soft/expansive clay with poor foundation-bearing capabilities.

VES4 shows the presence of 3 geoelectric layers. The basement is the second layer at a depth of 3m and is 50 m thick with resistivity 350-500 Ωm, an indication of compacted gravel with silt, sand, and clay, and has good foundation bearing capabilities. The top layer is 3 m thick with a resistivity of 20-40 Ωm, indicating soft/expansive clay with poor foundation-bearing capabilities.

VES5 shows the presence of 3 geoelectric layers, the basement being the third layer at a depth of 2 m with resistivity values 50-100 Ωm, indicating the shallow clayey basement with poor foundation bearing capabilities. The second layer is at a depth of 1m. It is 1m thick with a resistivity of 5000-8500 Ωm, indicating a thin shallow compact sub-basement with good bearing capabilities. The top layer is 1m thick with a resistivity of 5-15 Ωm, showing soft/expansive clay with poor foundation bearing capabilities.

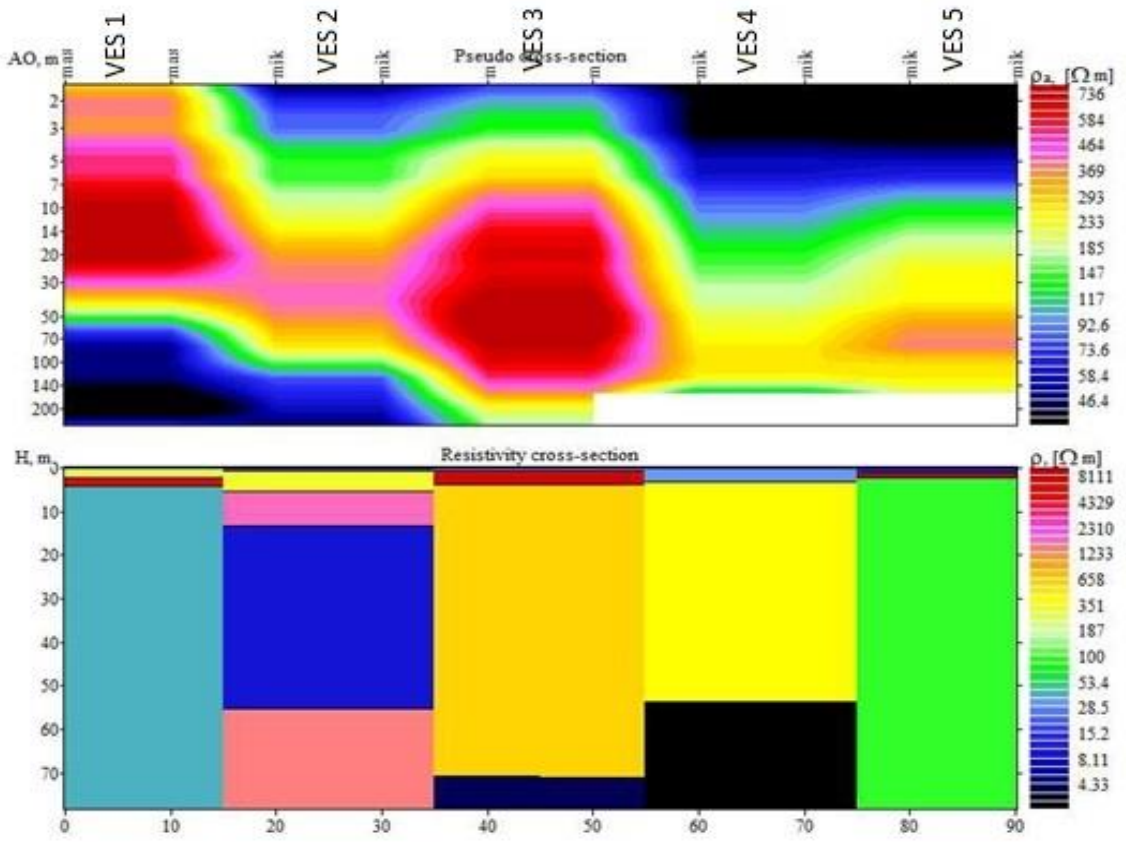

Figure 4: Pseudo and resistivity cross-section for VES 1-5.

Pseudo and resistivity cross-sections for VES6, VES7, VES8, VES9, and VES10 are shown in Figure 5. VES6 shows the presence of 4 geoelectric layers. The basement is the third layer at a depth of 7 m and is 55 m thick with resistivity values 1000-1500 Ωm, indicating a compact basement with good foundation-bearing capabilities. The second layer is at a depth of 0.5 m. It is 7 m thick with resistivity values 70-100 Ωm, indicating a compacted alluvium deposit with clay with moderate to good foundation bearing capabilities. The top layer is 0.5 m thick with resistivity values of 40-50 Ωm, showing soft/expansive clay with poor foundation bearing capabilities.

VES7 shows the presence of 5 geoelectric layers, the basement being the fourth layer at a depth of 20 m and is 18 m thick with resistivity values 10-25 Ωm, an indication of a highly fractured/weathered and saturated basement that has poor foundation bearing capabilities. The third and the second layer are at a depth of 0.3m. They are 4 m and 16 m thick, respectively, with resistivity values of 200-350 Ωm and 350-500 Ωm, respectively, an indication of gravel and sand which has moderate to good foundation bearing capabilities. The top layer is 0.3 m thick with resistivity values of 120-140 Ωm, an indication of alluvium deposit with clay which has poor foundation bearing capabilities.

VES 8 shows the presence of 3 geoelectric layers. The basement is the third layer at a depth of 10 m with resistivity values of 40-50 Ωm, indicating a weathered basement with poor bearing capabilities. The second layer of VES 8 is at a depth of 4 m and is 6 m thick with resistivity values 1000-1700 Ωm, indicating a compact sub-basement with good foundation bearing capabilities. The top layer is 4m thick with a resistivity of 10-30 Ωm, showing soft/expansive clay with poor foundation bearing capabilities.

VES 9 shows the presence of 3 geoelectric layers. The basement is the second layer at 14 m with a resistivity value of 500-800 Ωm, indicating gravel and alluvium deposits with moderate to good foundation bearing capabilities. The top layer is 14m thick with a resistivity value of 40-60 Ωm, showing soft clay and loose alluvium deposits with poor foundation bearing capabilities.

VES10 shows the presence of 3 geoelectric layers. The established basement was the second layer at a depth of 0.4 m. It is 120m thick with resistivity values 700-900 Ωm, depicting compacted gravel and sand with good foundation bearing capabilities. The topmost layer is 0.4 m thick with resistivity values of 2-10 Ωm, showing soft/expansive clay with poor foundation bearing capabilities.

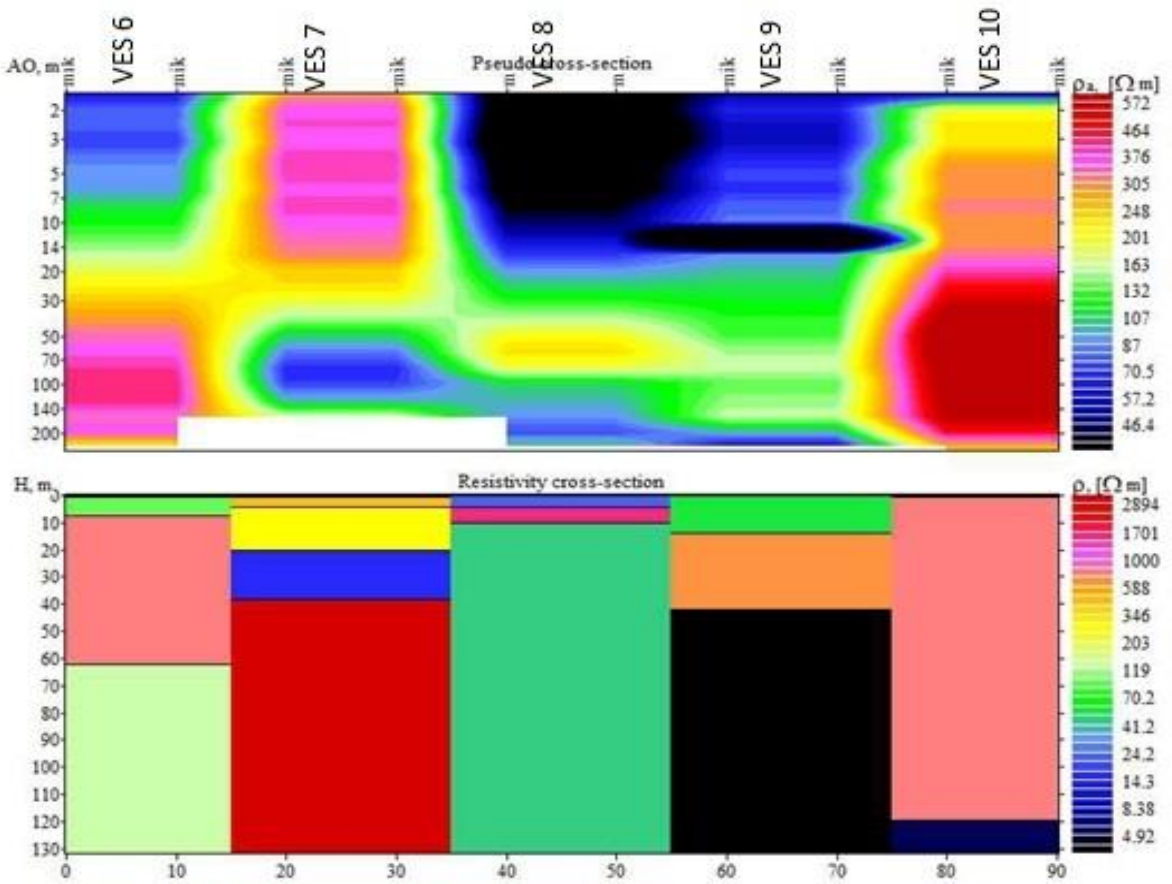

Figure 5: Pseudo and resistivity cross-section for VES 6-10.

3.3 Summary of VES data interpretation

Tables 1, 2, and 3 shows a summary of VES 1-10 data interpretation.

Table 1: Summary of VES 1-3 data interpretation.

SOUNDING NUMBER	LAYERS	RESISTIVITY (Ωm)	THICKNESS (m)	DEPTH (m)	CURVE TYPE	PROBABLE LITHOLOGY
VES 1	1	200	2.15	2.15	K-Type $\rho_1 < \rho_2 > \rho_3$	Alluvium-clay Compact zone saturated zone
	2	5005	2.06	4.2		
	3	35.5				
VES 2	1 2 3	19.6 783 41.7	0.648 18.7	0.648 19.4	K-Type $\rho_1 < \rho_2 > \rho_3$	Soft clay Gravel-sand Fractured
VES 3	1 2 3 4	33.1 7621 657 3.79	0.68 3.02 67.1	0.68 3.7 70.8	K-Type $\rho_1 < \rho_2 > \rho_3 > \rho_4$	Soft clay Compact zone Gravel-sand Saturated zone

Table 2: Summary of VES 4-6 data interpretation.

SOUNDING NUMBER	LAYERS	RESISTIVITY (Ωm)	THICKNESS (m)	DEPTH (m)	CURVE TYPE	PROBABLE LITHOLOGY
VES 4	1 2 3	32.6 400 1.6	3.13 50.5	3.13 53.7	K-Type $\rho_1 < \rho_2 > \rho_3$	Soft clay Alluvium-gravel Saturated zone
VES 5	1 2 3	11.7 16516 82.9	1.03 1.26	1.03 2.29	K-Type $\rho_1 < \rho_2 > \rho_3$	Soft clay Compact zone Alluvium clay
VES 6	1 2 3 4	37.6 92.6 737 123	0.445 6.01 55	0.445 6.45 61.45	KH-Type $\rho_1 < \rho_2 < \rho_3 > \rho_4$	Soft clay Alluvium-clay Gravel-sand

Table 3: Summary of VES 7-10 data interpretation.

SOUNDING NUMBER	LAYERS	RESISTIVITY (Ωm)	THICKNESS (m)	DEPTH (m)	CURVE TYPE	PROBABLE LITHOLOGY
VES 7	1 2 3 4 5	133 466 271 15.6 19572	0.328 3.86 15.8 18.1	0.328 4.18 20.0 38.1	K-Type $\rho_1 < \rho_2 > \rho_3$	Alluvium-clay Gravel-sand Alluvium-gravel Saturated zone Compact zone
VES 8	1 2 3	21.4 1643 46	4.08 5.93	4.08 10	K-Type $\rho_1 < \rho_2 > \rho_3$	Soft clay Compact zone Fractured zone
VES 9	1 2 3	55.6 604 0.792	13.9 28	13.9 41.9	K-Type $\rho_1 < \rho_2 > \rho_3$	Alluvium-clay Gravel-sand Saturated zone
VES 10	1 2 3	22.8 739 5.86	0.339 119	0.339 119	K-Type $\rho_1 < \rho_2 > \rho_3$	Soft clay Gravel-sand Saturated zone

3.4 The First break picks

Figure 6 shows a section of the 24-channel refraction record with the first break picks indicated along the red line for spread 1 first shot point -1.5 m from the first geophone. The first and last shot break pick for seismic spreads 1, 2 and 3 were used in the Seisimager Plotrefa window to generate the forward and reverse travel time curves as shown in Figures 15, 16, and 17 from which 2D seismic spread models in Figures 18, 19, and 20 were generated. Other first break picks are shown in Figures 7, 8, 9, 10, 11,12, 13 and 14.

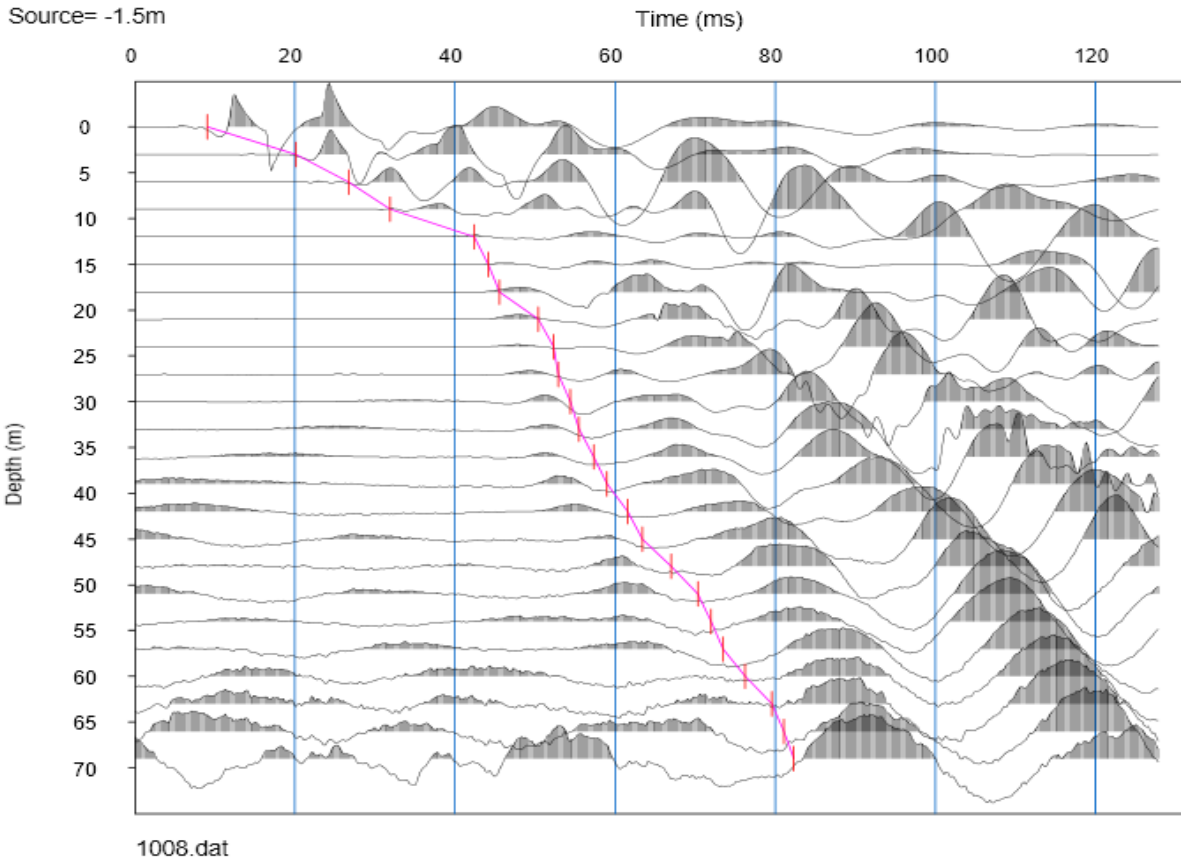

Figure 6: First shot, the first break picks spread 1.

Figure 7 shows a section of the 24-channel refraction record with the first break picks indicated along the red line for spread 1 mid shot point 34.5 m from the first geophone.

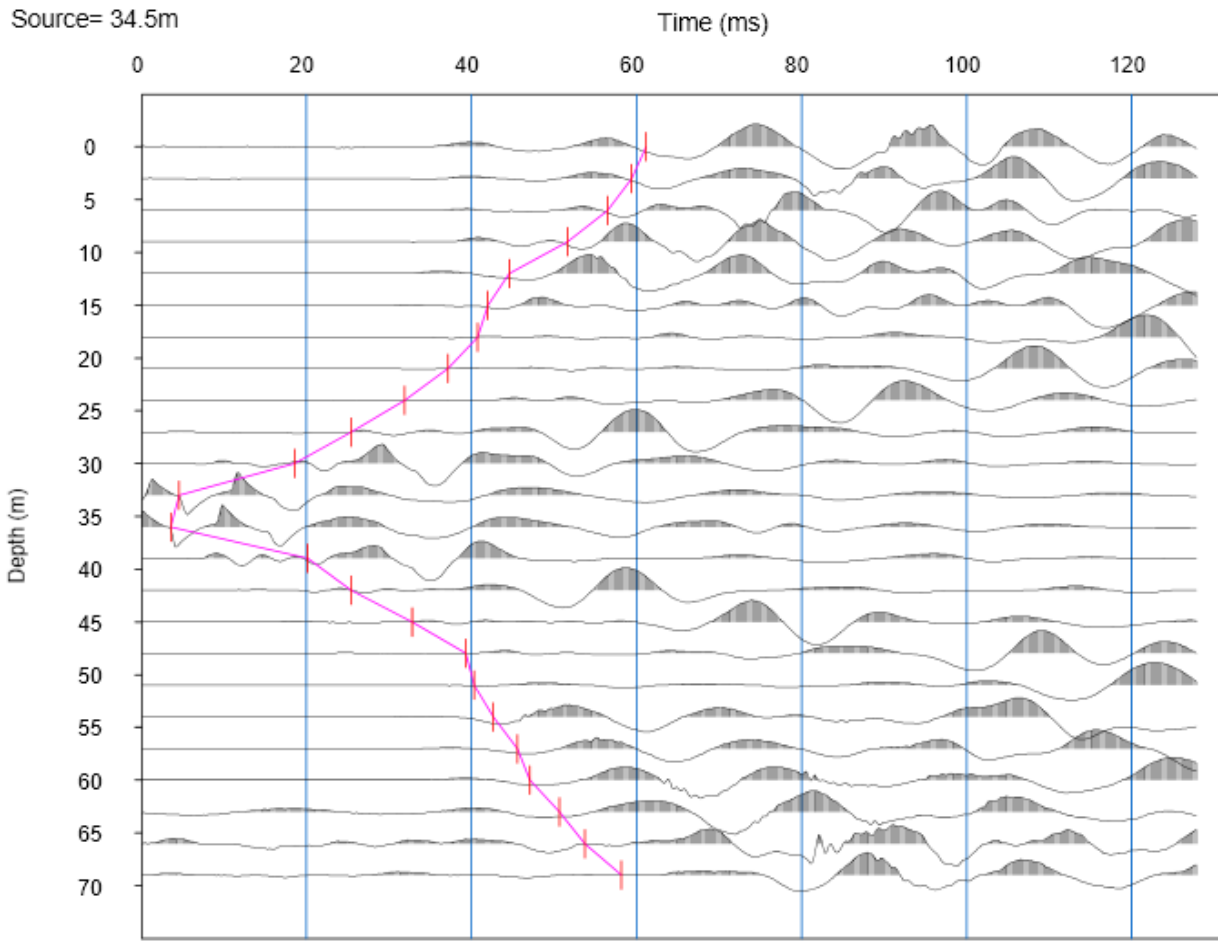

Figure 7: Mid shot, the first break pick spread 1.

Figure 8 shows a section of the 24-channel refraction record with the first break picks indicated along the red line for spread 1 last shot point 67.5 m from the first geophone.

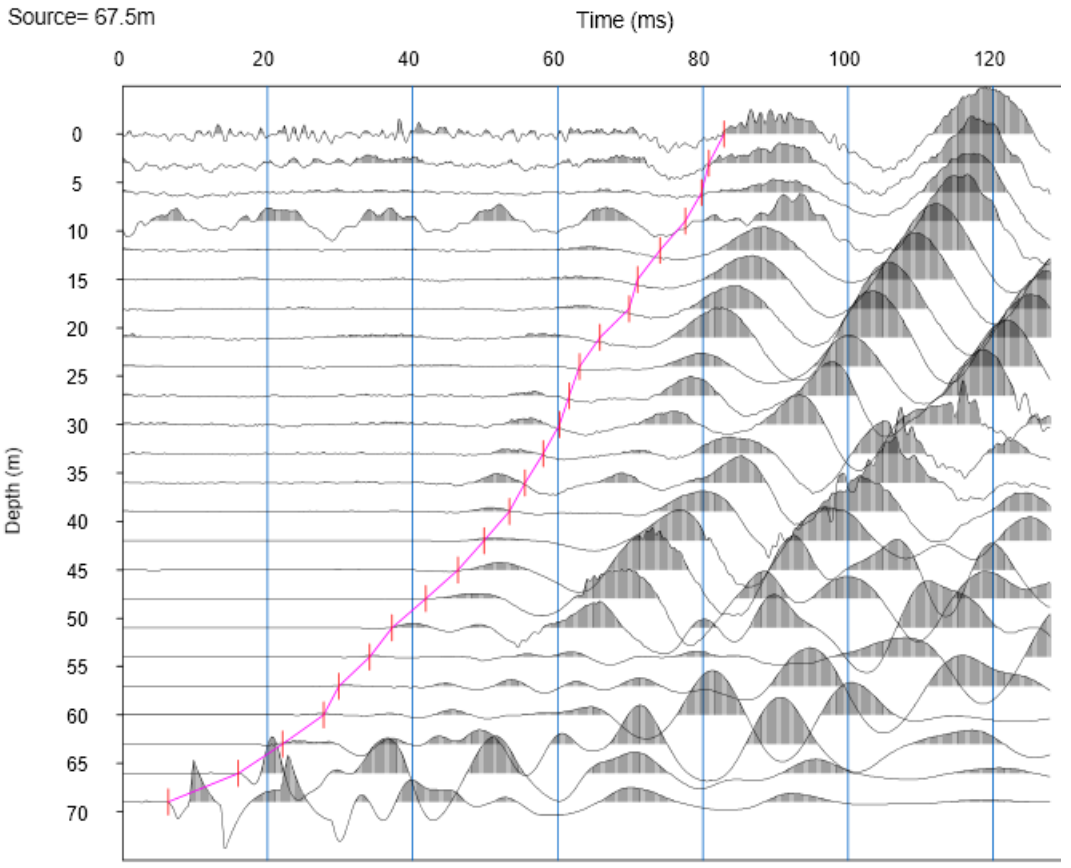

Figure 8: Last shot, the first break picks spread 1.

Figure 9 shows a section of the 24-channel refraction record with the first break picks indicated along the red line for spread 2 first shot point -1.5 m from the first geophone.

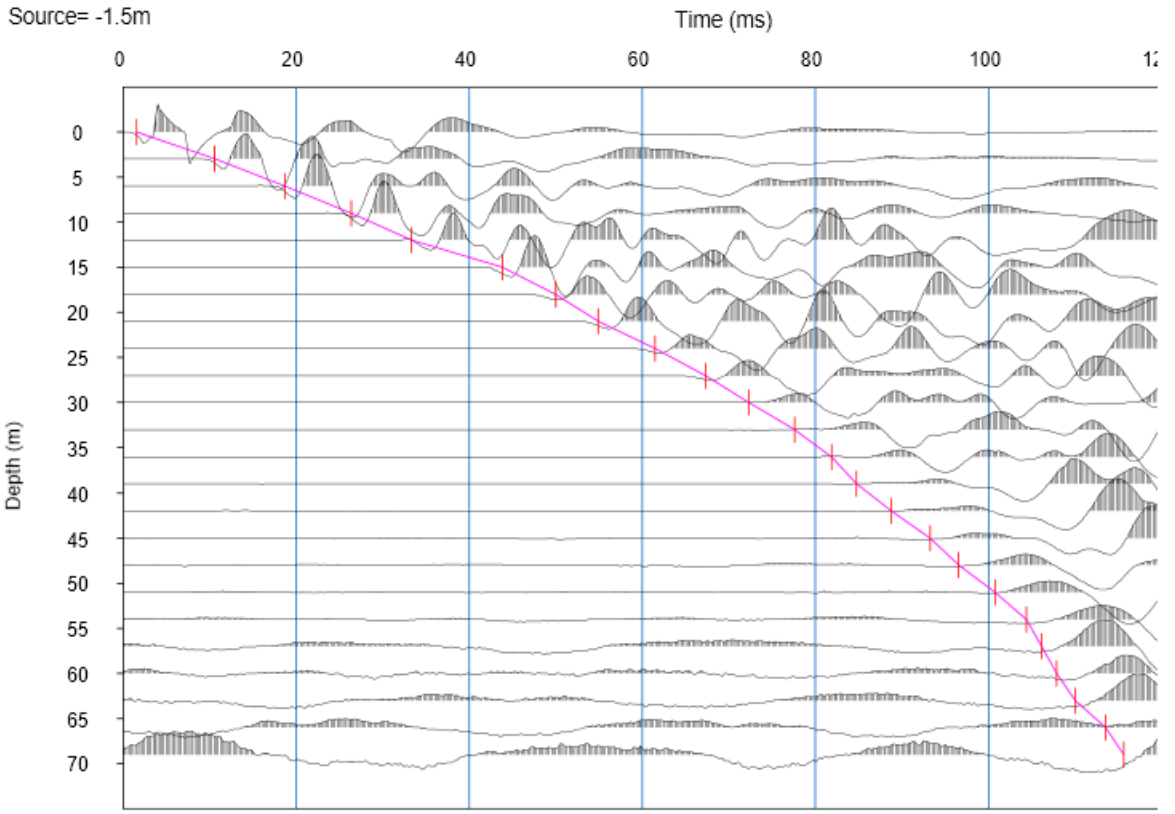

Figure 9: First shot, the first break picks spread 2.

Figure 10 shows a sample data section of a 24-channel refraction record with the first break picks indicated along the red line for the spread of two mid-shot points 34.5 m from the first geophone.

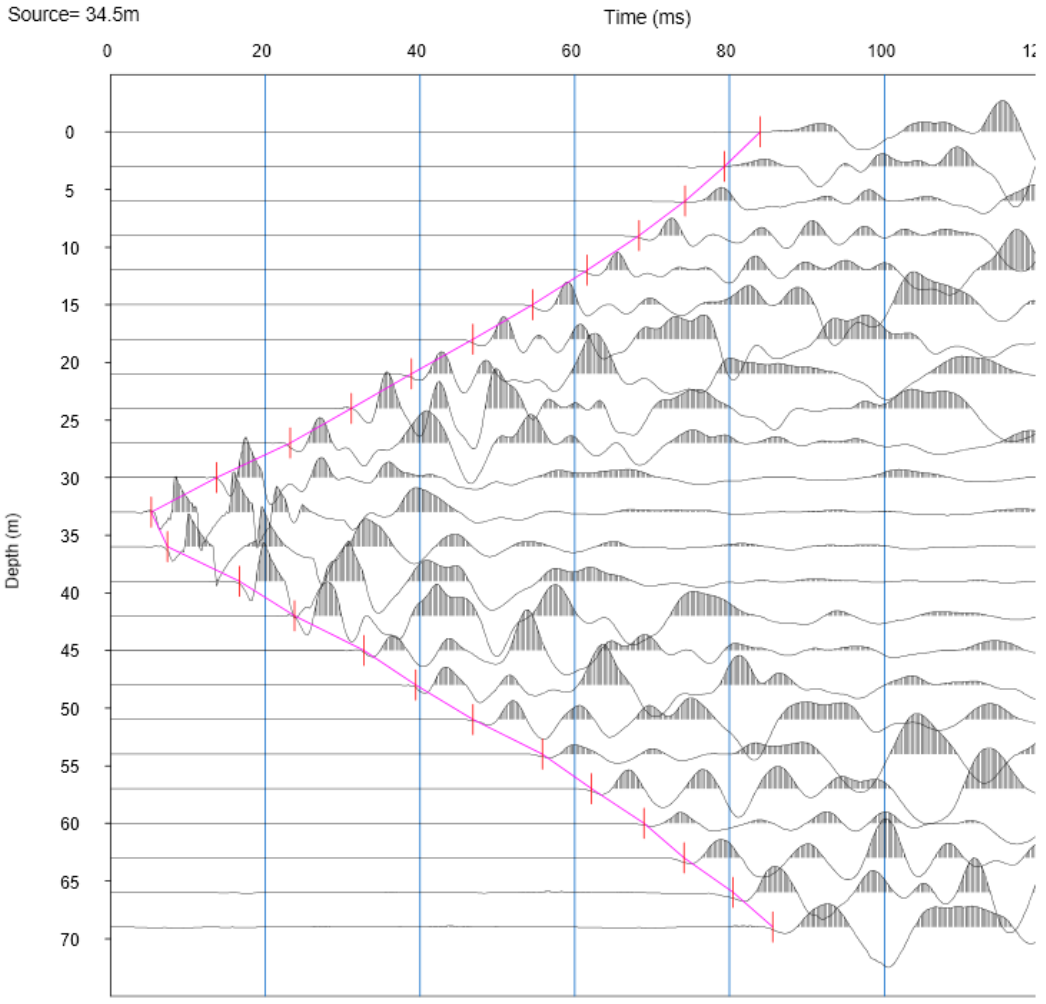

Figure 10: Mid-shot first break picks spread 2.

Figure 11 shows a section of the 24-channel refraction record with the first break picks indicated along the red line for spread 2 last shot point 67.5m from the first geophone.

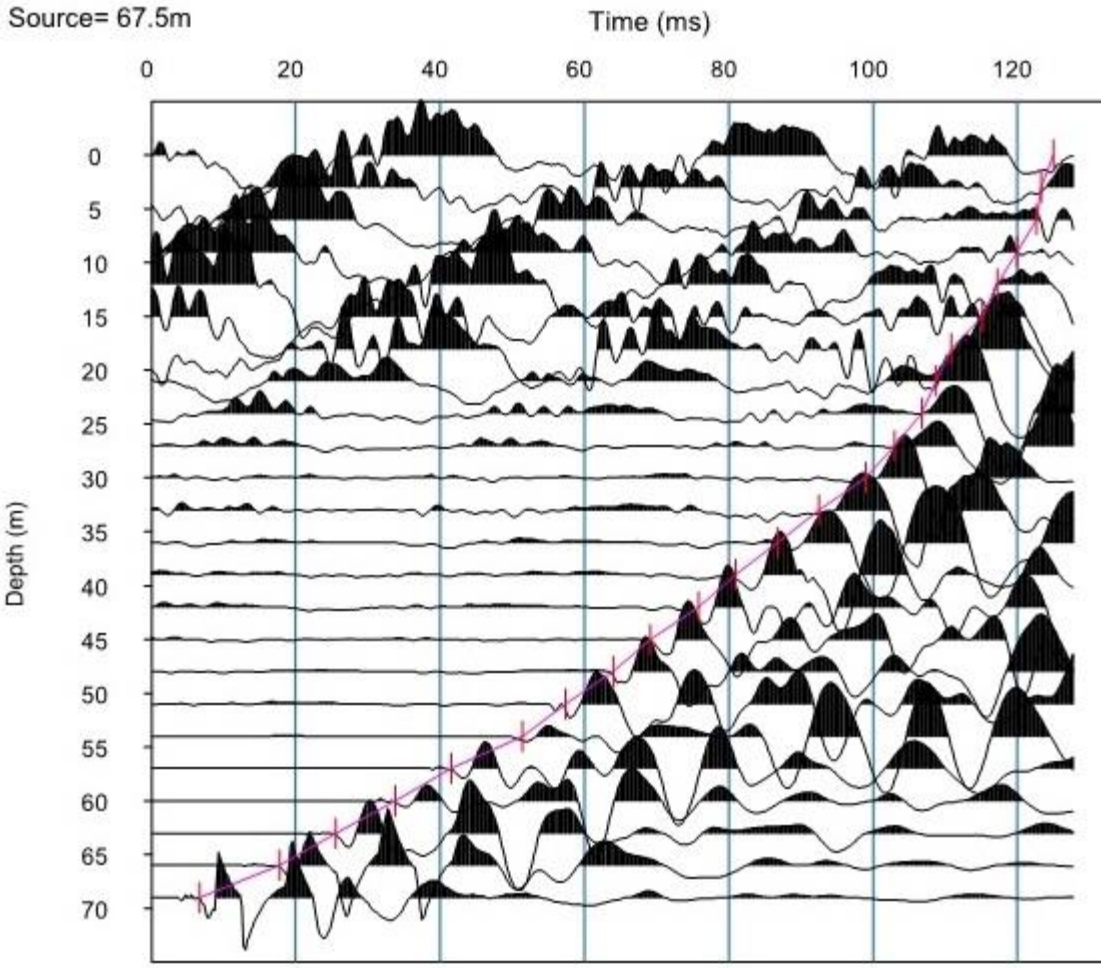

Figure 11: Last shot, the first break picks spread 2.

Figure 12 shows a section of the 24-channel refraction record with the first break picks indicated along the red line for spread 3 first shot point -1.5 m from the first geophone.

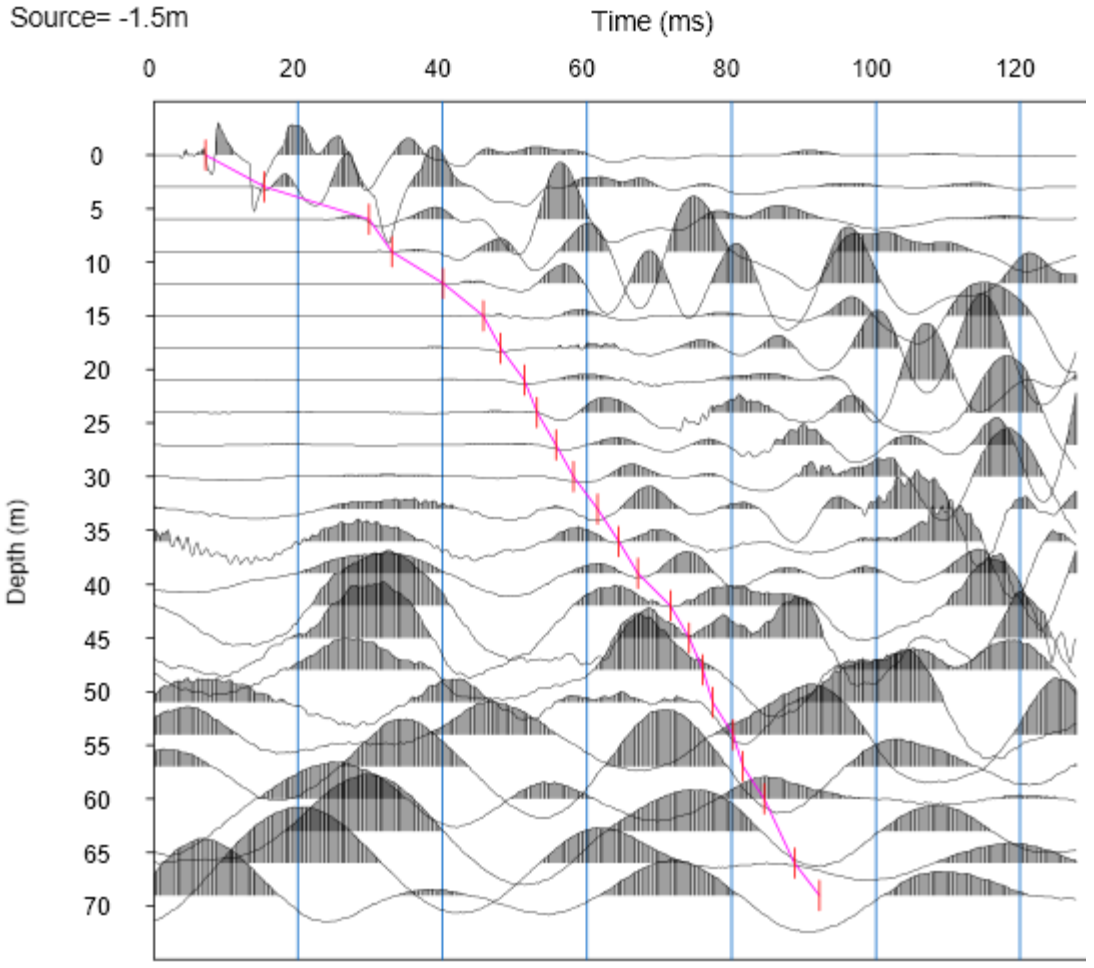

Figure 12: First shot, the first break picks spread 3.

Figure 13 shows a section of the 24-channel refraction record with the first break picks indicated along the red line for spread 3 mid shot point 34.5m from the first geophone.

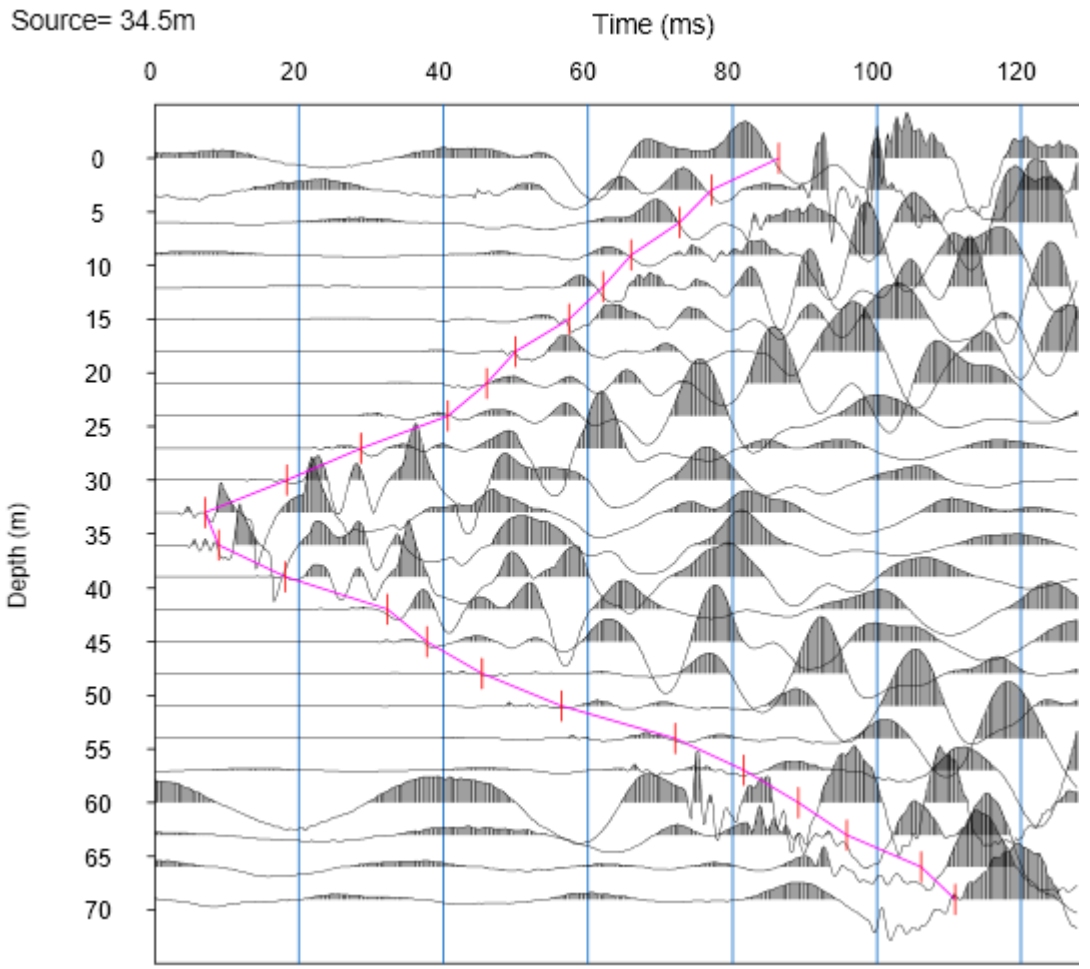

Figure 13: Mid-shot first break picks spread 3.

Figure 14 shows a section of the 24-channel refraction record with the first break picks indicated along the red line for spread 3 last shot point 70.5m from the first geophone.

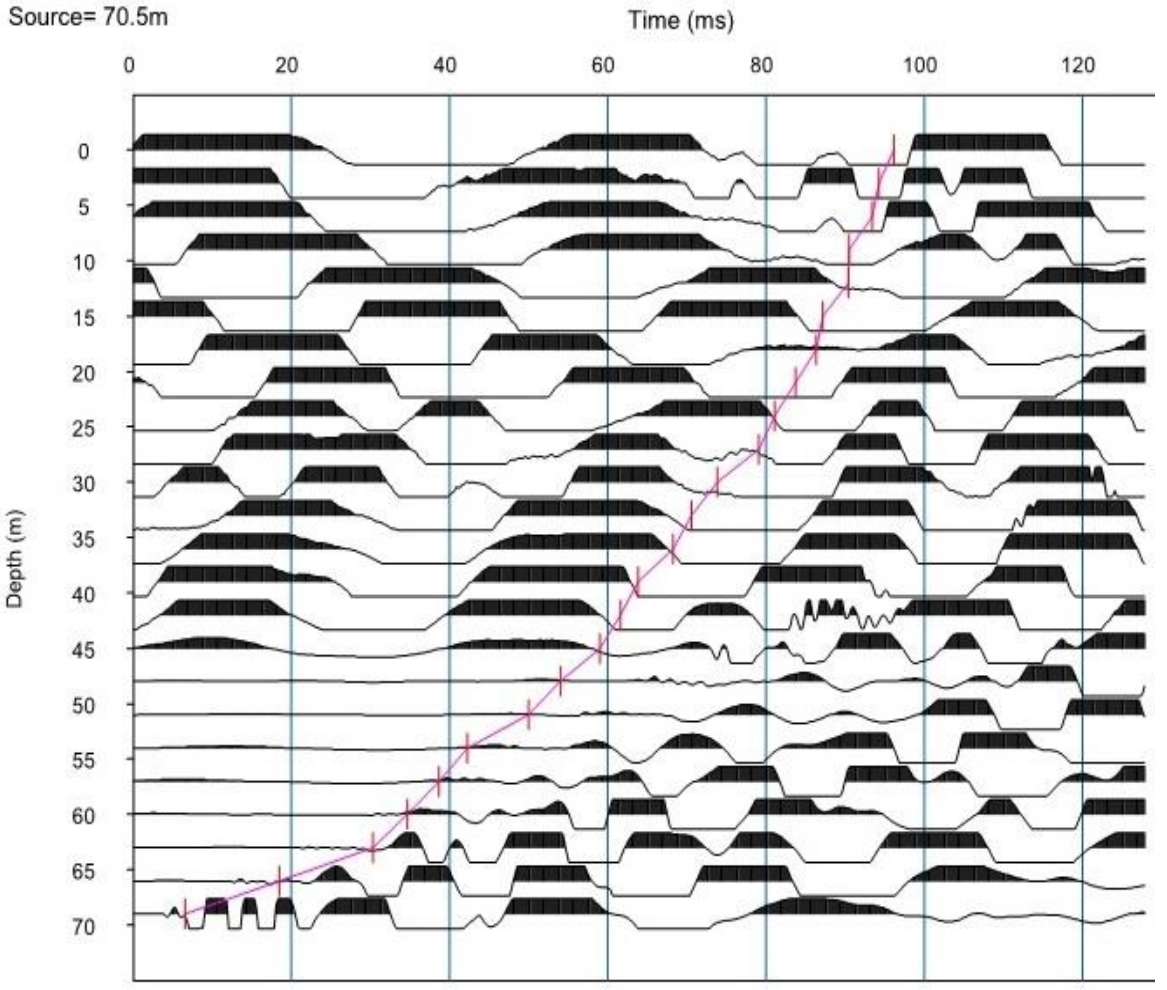

Figure 14: Last shot, the first break picks spread 3.

3.5 Travel time curves

The forward and reverse travel time curves in Figure 15 show the presence of three geologic layers to a depth of 35 m that was investigated. The first layer represents loose top soils, mostly clay and alluvium deposits, to a maximum depth of 2.69 m in the dip end and 1.7 m in the shallow end, with poor foundation bearing capabilities. The reverse shot is vital in determining the dipping, especially when the interface is dipping at more than 10% (Waryszak et al., 2021). This layer dips at an approximate angle of 12.7^0 from the southwest to the northeast direction, the direct wave velocity of this layer is approximately 303 m/s. The second layer has refracted wave velocity of 429 m/s. This velocity comprises weathered rock,

compact lateritic and saprolitic materials, and kunkar silts from a depth of 1-3 m. The basalt layer has a refracted wave velocity of 1000 m/s. This value is typical of soft, weathered rock olivine basalts at varying water saturation levels (Emmanuel, 2015).

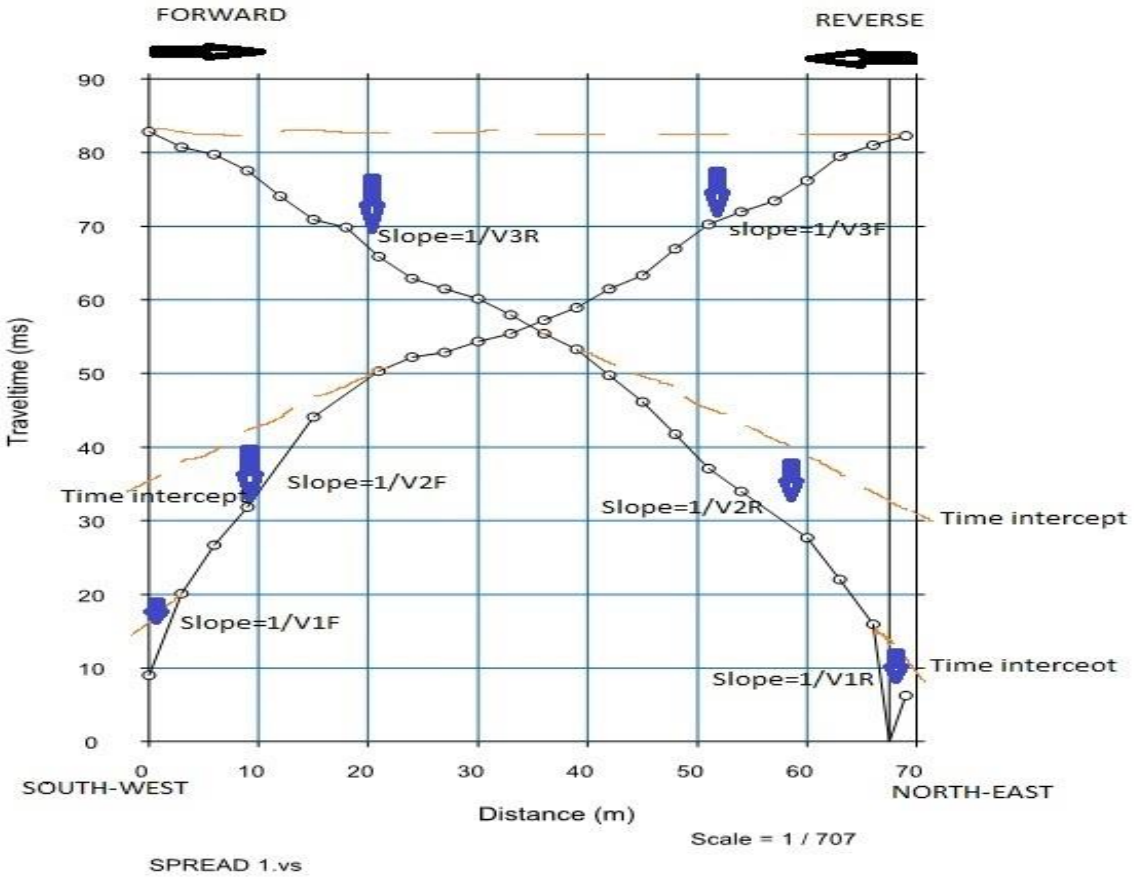

Figure 15: Travel time curves spread 1 (forward and reverse traverse).

The forward and reverse travel time curves in Figure 16 show the presence of three geologic layers to a depth of 35 m that was investigated. The first layer represents loose top soils, mostly clay and alluvium deposits, to a maximum depth of 4.02 m in the dip end and 2.23 m in the shallow end, with poor foundation-bearing capabilities. The layer dips at an angle of approximately 3.8^0 from the southwest to the northeast direction, the direct wave velocity of this layer is approximately 345 m/s. The second layer has refracted wave velocity of 600 m/s. The velocity value indicates weathered rock, compact lateritic and saprolitic materials, and kunkar silts from a depth of 2-4 m. The basalt layer has a refracted wave velocity of 1111 m/s. This value indicates soft, weathered rock olivine basalts and a possible water table.

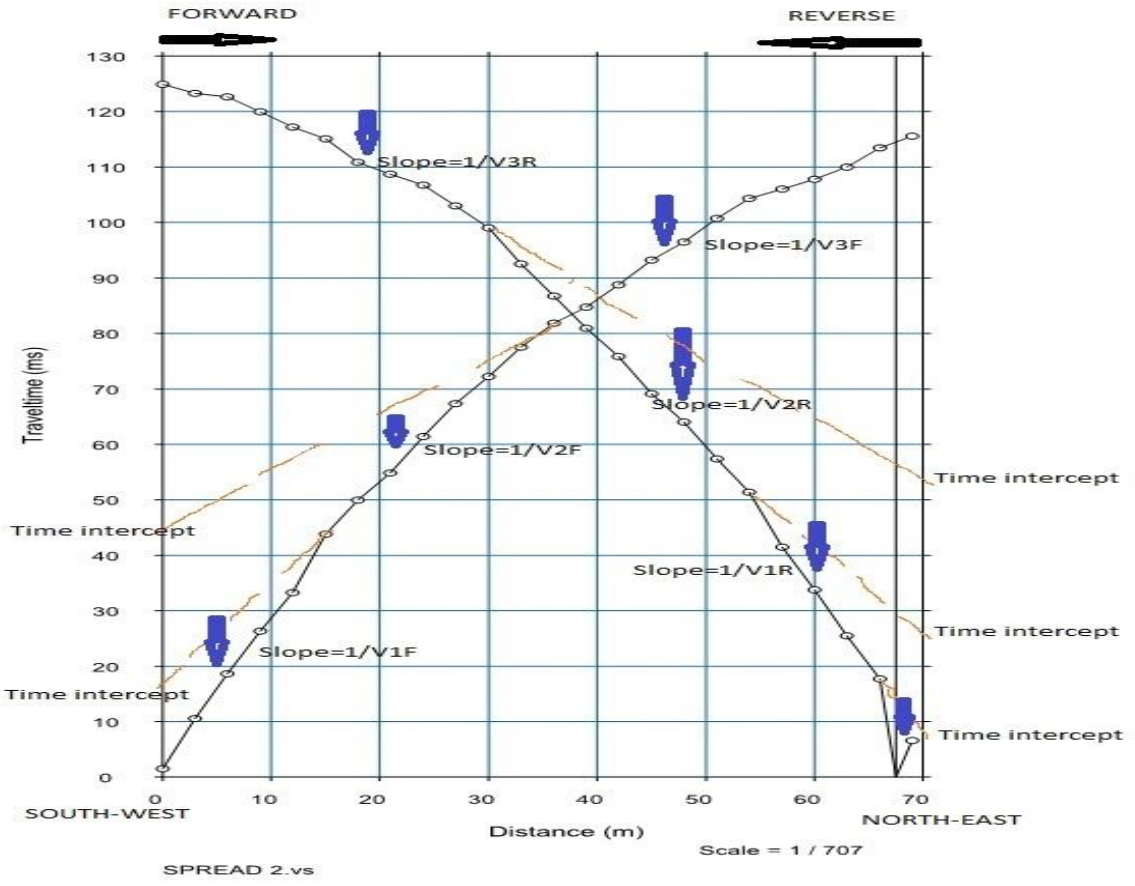

Figure 16: Travel time curves spread 2 (forward and reverse traverse).

The forward and reverse travel time curves in Figure 17 shows the presence of three geologic layers to a depth of 35 m probed. The first layer represents loose top soils, mostly clay and alluvium deposits, to a maximum depth of 6.75 m in the dip end and 4.5 m in the shallow end, with poor foundation-bearing capabilities. This layer dips at a slight angle of approximately 8.1^0 from the northeast to southwest direction, since the intercept time of the second layer for the reverse curve 25 ms is less than the intercept time for the forward curve 30ms, as shown in Figure 17; the velocity of this layer is approximately 409 m/s. The second layer has an estimated velocity of 1111 m/s in the up-dip and 667 m/s in the down-dip direction, calculated from the forward and reverse waves, respectively, from Figure 17. This velocity indicates weathered rock, compact lateritic and saprolitic materials, and kukar silts from a depth of 4-7 m. The basalt layer has a velocity of 1500 m/s. This value indicates soft, weathered rock olivine basalts and a possible water table (Emmanuel, 2015).

The estimated cross-over distances are 9.17 m and 4.14 m in the down-dip (forward) and up-dip (reverse) directions, respectively, with the geophone spacing distance at 3 m and the shot points at 1.5 m from the first geophone. This cross-over distance shows that the first break pick for the first three geophones in the forward direction was due to the direct wave and only the last geophone in reverse. The rest of the first break picks emanated from the refracted waves.

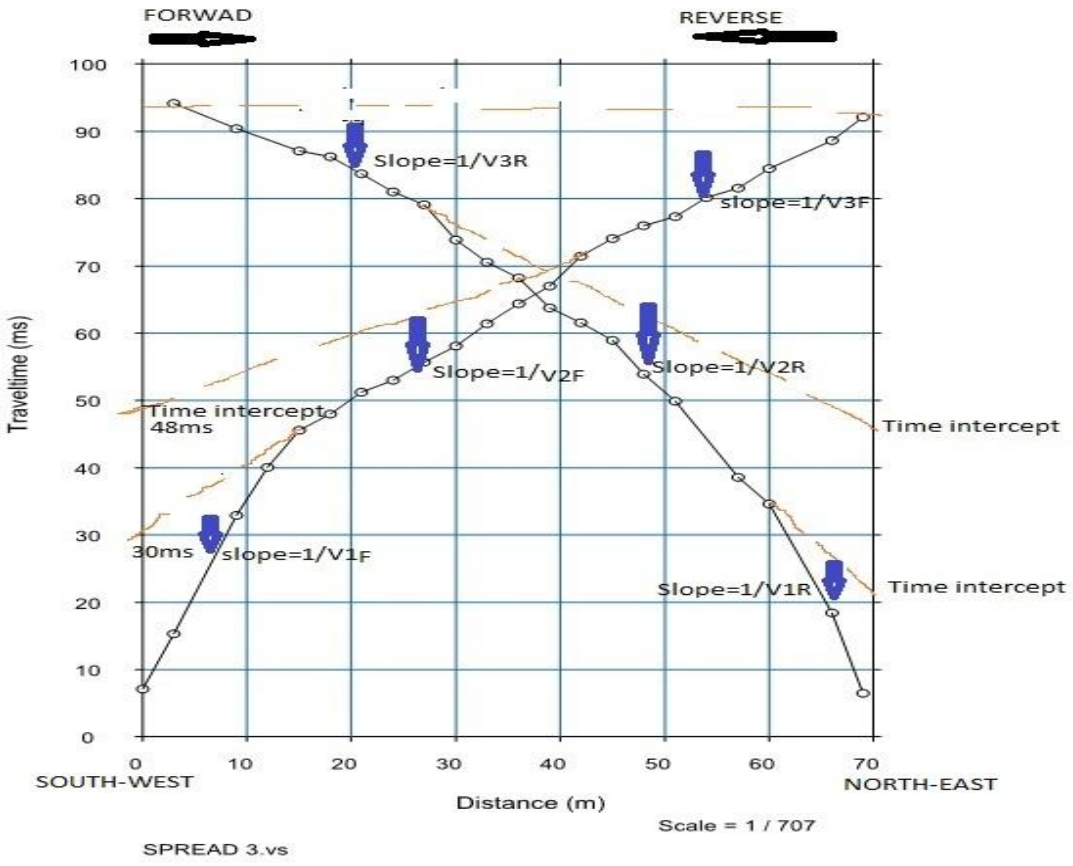

Figure 17: Travel time curves spread 3 (forward and reverse traverse).

3.6 2-D Seismic spread models

The model in Figure 18 depicts three acoustic layers with varying depths; similarly, the ten VES points also revealed three geoelectric layers to a depth of 35 m, as shown in tables 1, 2, and 3. The p- velocities for the acoustic layers range from 250 m/s to > 3000 m/s. The first layer represents loose top soils, mostly clay and alluvium deposits, to a maximum depth of 3.5 m. The velocity range of this layer is 250-450 m/s and is represented by the pinkish colour in the model. The second layer has velocities between 500-1500 m/s. This velocity comprises weathered rock, compact lateritic and saprolitic materials, and kurkar silts from a depth of 4-10 m to 5-15 m. This layer is shown in red-yellowish. The basalt layer starts at a depth of 15-20 m recording velocities from 1500 m/s to > 3000 m/s. These values are typical of soft, weathered rock olivine basalts at varying levels of water saturation.

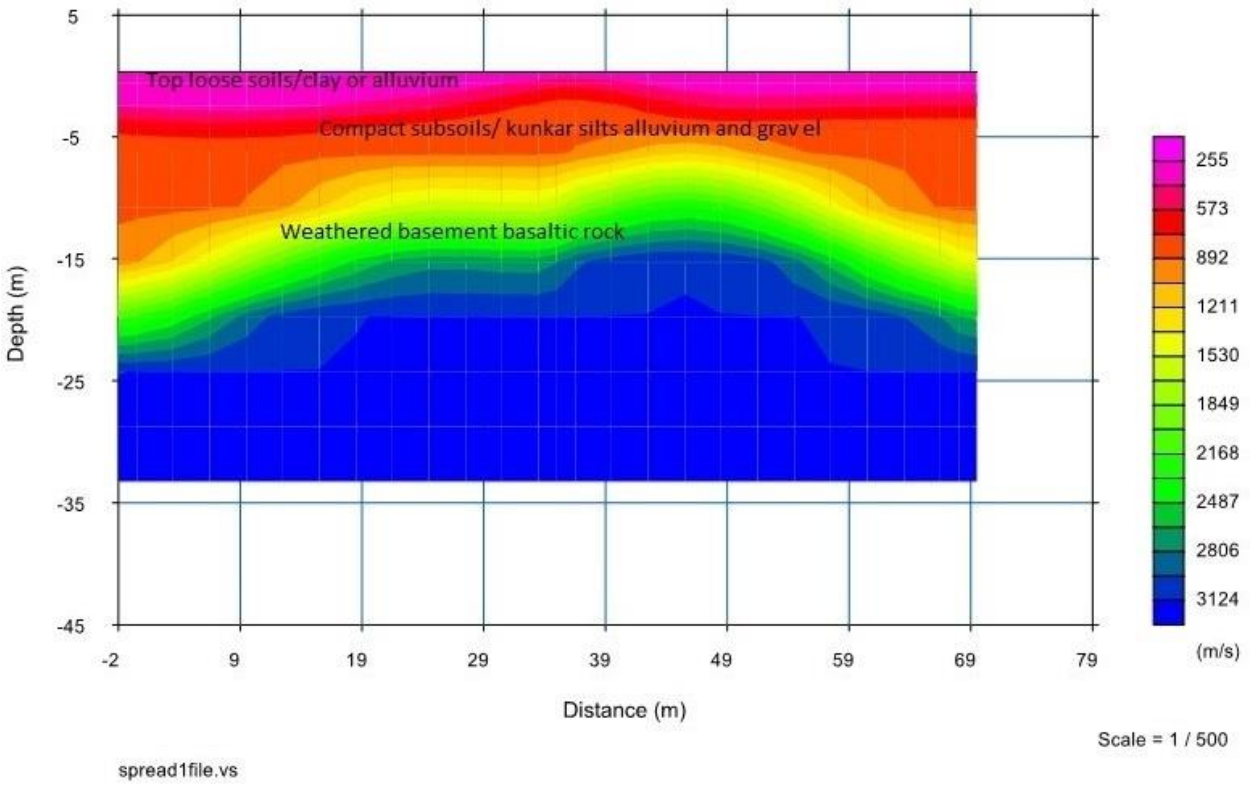

Figure 18: Seismic 2D Model for Spread 1.

The model in Figure 19 reveals three layers with varying depths with p- velocities ranging from 250 m/s to > 700 m/s. The first layer represents loose top soils, mostly clay and alluvium deposits, to a maximum depth of 4m. The velocity range of this layer is 250-450 m/s. The second layer has velocities between 500-600 m/s. These velocity values comprise weathered rock, compact lateritic and saprolitic materials, and kurkar silts from a depth of 4-10 m to 5-15 m. The basalt layer starts at a depth of 15-20 m recording velocities from 650 m/s to > 700 m/s. These values are typical of soft, weathered rock (olivine basalts).

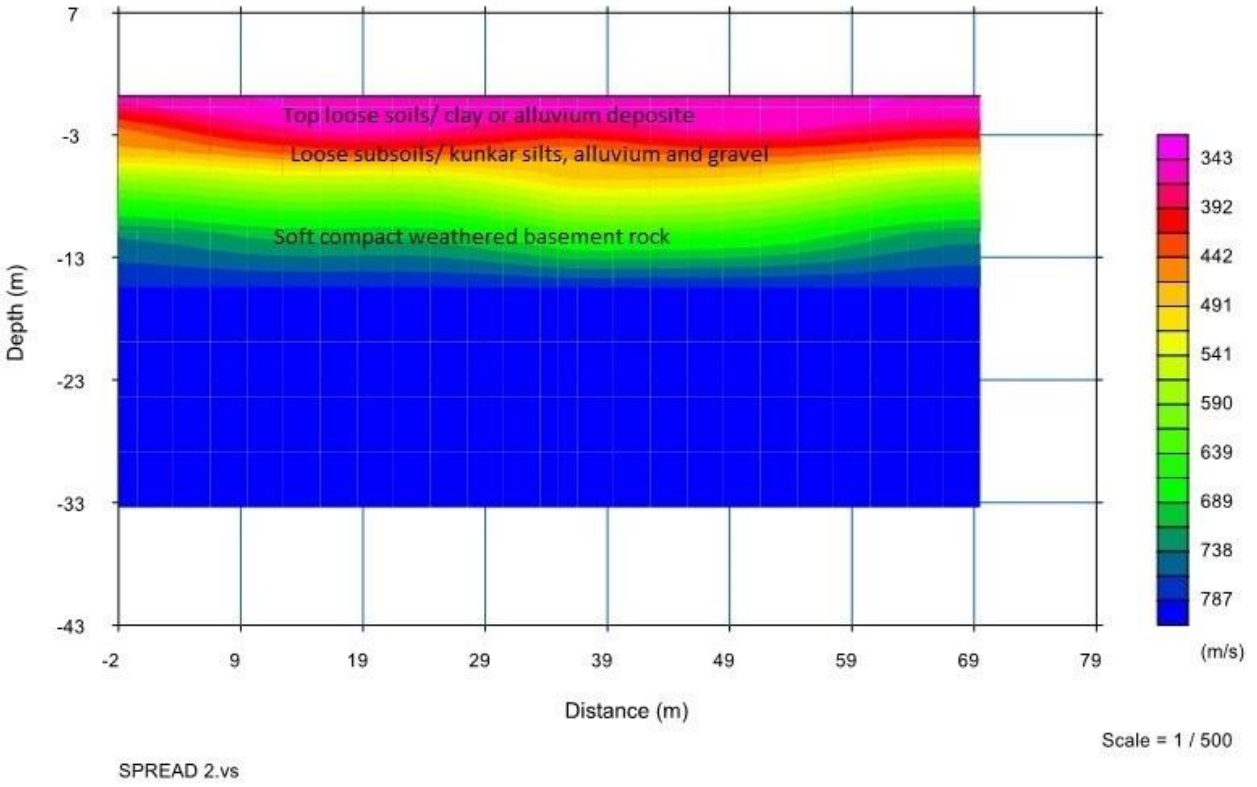

Figure 19: Seismic 2D Model for Spread 2.

The model in Figure 20 shows three layers with varying depths with p- velocities ranging from 200 m/s to > 1300 m/s. The first layer represents loose top soils, mostly clay and alluvium deposits to a maximum depth of 3 m, with poor foundation-bearing capabilities. The velocity range of this layer is 200-300 m/s. The second layer has velocities between 300-800 m/s. This velocity typically comprises weathered rock and loose to compact lateritic and saprolitic materials and kurkar silts from 2-5 m to 2-25 m. The basement starts at a depth of 5-25 m recording velocities from 800 m/s to > 1300 m/s. These values are typical of soft, weathered rock (olivine basalts).

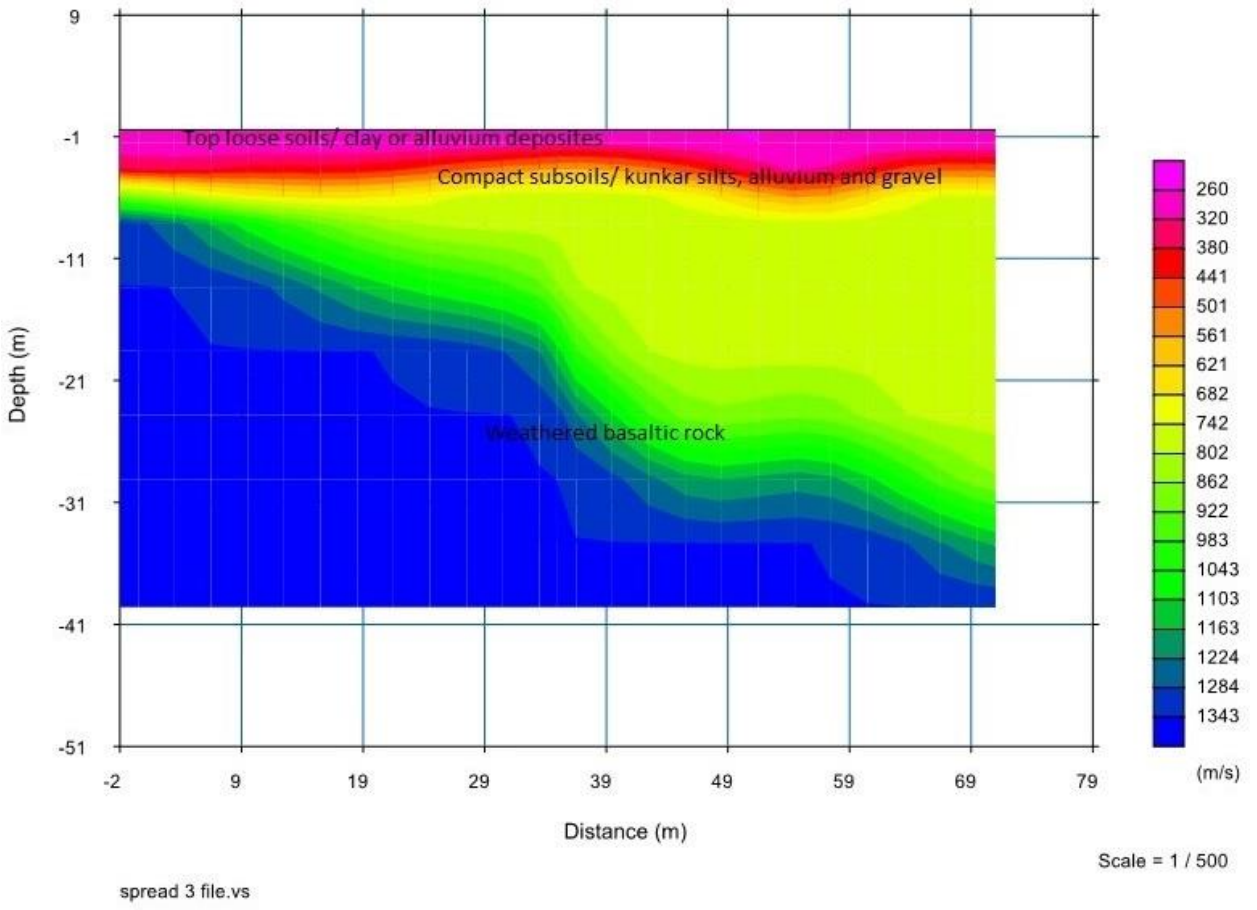

Figure 20: Seismic 2D Model for Spread 3.

3.7 Geologic structures mapped

Further modelling involved data export from pseudo and resistivity cross-section to Surfer software from which a 2D contour map was generated showing a cross section to a depth of 250 m, as shown in Figures 21 and 22. Figure 21 shows the suspected intrusion extending to the near surface at the central region and downward to a depth of about 150m. The suspected intrusion has a resistivity value of 500-1050 Ωm and is surrounded by a 100-300 Ωm matrix.

A suspected normal fault to the east buried at a depth of 50m and extending to unknown depth with a resistivity value of 1-100 Ωm is noted and is surrounded by a 300 Ωm matrix. The low resistivity value of the fault indicates that it is saturated.

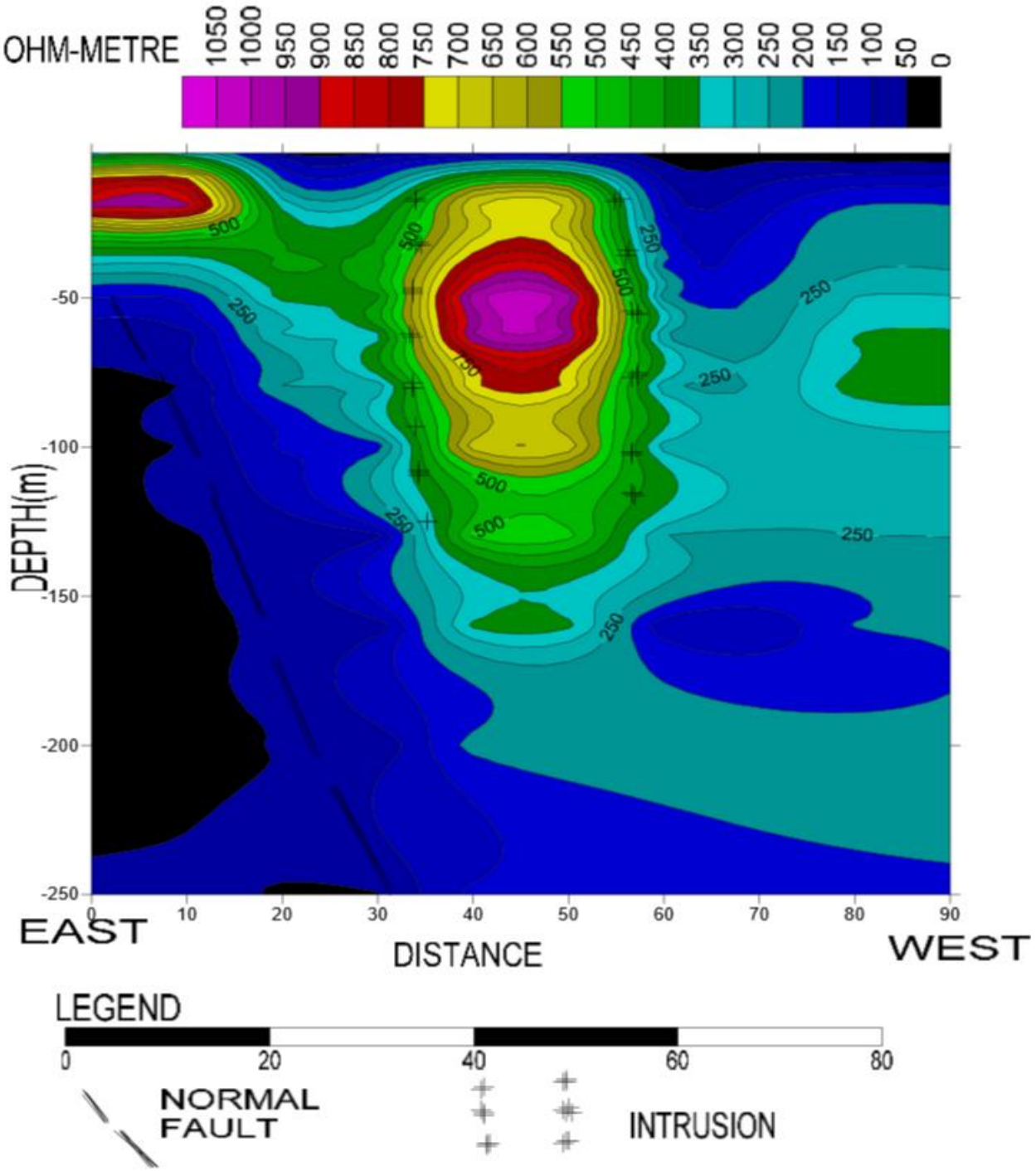

Figure 21: Apparent resistivity surfer pseudo-cross-section based on VES 1-5.

Figure 22 shows a suspected normal fault also buried at a depth of 50m, extending to unknown depth with a resistivity value of 1-100 Ωm and surrounded by a 300-500 Ωm matrix. The fault is highly fractured and saturated.
An intrusion is suspected on the far east and west extending near to the surface with resistivity value of 500-900 Ωm and is surrounded by 200-300 Ωm matrix.

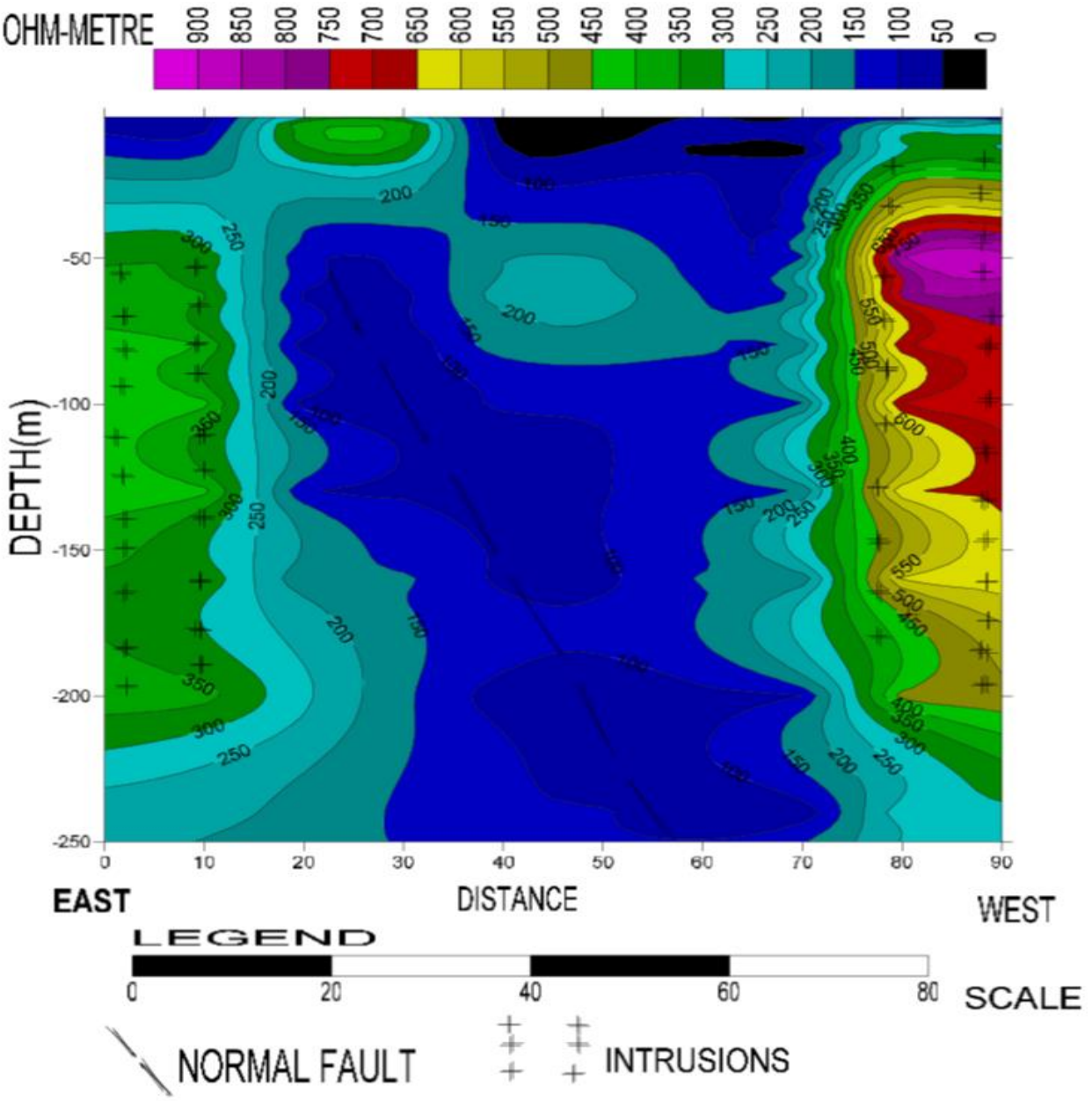

Figure 22: Apparent resistivity surfer pseudo-cross-section based on VES 6-10.

4. Conclusion

Electrical resistivity and seismic refraction techniques have been employed to investigate and characterize the subsurface at Mikinduri town in Meru County, Kenya. Based on Wenner profiling, with ten VES, and the seismic survey that was carried out, three significant layers were delineated at Mikinduri town to a depth of 35 m; and up to 5 layers to a depth of 250 m. These layers comprised of loose clayey black cotton soil and alluvium deposits at the top layer, which are incompetent for bearing foundations. Compacted lateritic/saprolitic material and kurkar silts formed the second layer. And a soft, weathered, saturated basement and solid basaltic rock basement formed the third layer. The top layer is to a depth of 0.3 m in the southeast parts of the study area, to 13.9 m in the northern parts of the study area. The depth of a competent sub-basement bed ranges from 0.4 m to 15 m in the southern parts of the study area. The fractured, weathered, and saturated basement for underground water harvesting is identified between 65 m and 120 m in the northeast of the study area. Three acoustic layers were identified, with respective p-wave velocities of 250-450 m/s, 500-650 m/s, and 700-3300 m/s. Loose alluvium and clay soils have poor foundation bearing capabilities, while compacted gravel and hard basaltic rock basement have good foundation bearing capabilities.

References

[1] Abuga, V., Mustapha, K., Migwi, C., Ambusso, W.J. and Muthaka, G. (2013) Geophysical exploration of an iron ore deposit in Kimachia area in Meru County in Kenya, using gravity and magnetic technique. International Journal of Science and Research (IISR) 2 (11): 2319-7064.

[2] Andrews, N.D., Aning, A.A., Danour, S.K. and Noye, R.M. (2013). Geophysical investigation at the proposed site of the KNUST teaching hospital building using 2D and 3D resistivity imaging technique. International research journal of geology and mining (IRJGM) (2276-6618) Vol 3(3) pp 113-123, April 2013.

[3] Benson, M.C. (2016). Iron ore mineral deposits exploration by ground magnetic in Kindani Area, Meru County, Kenya. M.Sc. (Physics) thesis, Kenyatta University.

[4] Delgado, J., Lopez, C., Estevez, A., Giner, J., Cuenca, A. and Molina, S. (2000). Mapping soft soils in Segura River valley (S.E Spain): a case study of microtremors as an exploration tool. Journal of applied geophysics 45(2000) 19-32.

[5] Emmanuel, T. H. (2015). Geotechnical site investigation using seismic refraction and resistivity techniques. M.Sc. thesis, Kwame Nkrumah University of Science and Technology.

[6] Oluwakuse, O.A. and Adeyemo, I.A. (2020). Engineering geological investigation of pavement failure along Emure Ekiti-Akuyba Road Southwestern Nigeria. Asian Journal of geological research. 3(2):34-41, 2020; Article No AJOGER 57939.

[7] Mason, P. (1953). Geology of Meru-Isiolo area. Report No. 31. 1953.

[8] Waryszak, P., Gavoille, A., Whitt, A.A., Kelvin, J. and Macreadie, P.I. (2021). Combining gray and green infrastructure to improve coastal resilience: lessons learnt from hybrid flood defenses, Coastal Engineering Journal, 63:3, 335-350. DOI: 10.1080/21664250.2021.1920278.